

## Article

# Tribo-Mechanical Behavior of Films and Modified Layers Produced by Cathodic Cage and Glow Discharge Plasma Nitriding Techniques

Bruna C. E. Schibicheski Kurelo <sup>1,2,\*</sup>, Gelson Biscaia De Souza <sup>2</sup>, Silvio Luiz Rutz Da Silva <sup>2</sup>, Carlos Maurício Lepienski <sup>1</sup>, Clodomiro Alves Júnior <sup>3</sup>, Rafael Fillus Chuproski <sup>2</sup> and Giuseppe Pintaúde <sup>1</sup>

<sup>1</sup> Department of Mechanical Engineering, Federal Technological University of Paraná, Campus Ecoville, Curitiba 81280-34, Paraná, Brazil

<sup>2</sup> Laboratory of Mechanical Properties and Surfaces, Department of Physics, State University of Ponta Grossa, Campus Uvaranas, Ponta Grossa 84030-900, Paraná, Brazil

<sup>3</sup> Integrated Center for Technological Innovation of the Semi-arid Region, Federal Rural University of the Semi-Arid, Av. Francisco Mota 572, Mossoró 59625900, Rio Grande do Norte, Brazil

\* Correspondence: brunakurelo@utfpr.edu.br or bruna\_schibicheski@hotmail.com

**Abstract:** Two surface modification techniques, the glow discharge plasma nitriding (GDPN) and the cathodic cage plasma nitriding (CCPN), were compared regarding the mechanical and tribological behavior of layers produced on AISI 316 stainless-steel surfaces. The analyses were carried out at the micro/nanoscale using nanoindentation and nanoscratch tests. The nitriding temperature (°C) and time (h) parameters were 350/6, 400/6, and 450/6. Morphology, structure, and microstructure were evaluated by X-ray diffraction, scanning electron and optical interferometry microscopies, and energy-dispersive X-ray spectroscopy. GDPN results in stratified modified surfaces, solidly integrated with the substrate, with a temperature-dependent composition comprising nitrides ( $\gamma'$ -Fe<sub>4</sub>N,  $\epsilon$ -Fe<sub>2+x</sub>N, CrN) and N-solid solution ( $\gamma_N$  phase). The latter prevails for the low treatment temperatures. Hardness increases from ~2.5 GPa (bare surface) to ~15.5 GPa (450 °C). The scratch resistance of the GDPN-modified surfaces presents a strong correlation with the layer composition and thickness, with the result that the 400 °C condition exhibits the highest standards against microwear. In contrast, CCPN results in well-defined dual-layers for any of the temperatures. A top 0.3–0.8  $\mu\text{m}$ -thick nitride film (most  $\epsilon$ -phase), brittle and easily removable under scratch with loads as low as 63 mN, covers a  $\gamma_N$ -rich case with hardness of 10 GPa. The thickness of the underneath CCPN layer produced at 450 °C is similar to that from GDPN at 400 °C (3  $\mu\text{m}$ ); on the other hand, the average roughness is much lower, comparable to the reference surface (Ra ~10 nm), while the layer formation involves no chromium depletion. Moreover, edge effects are absent across the entire sample's surface. In conclusion, among the studied conditions, the GDPN 400 °C disclosed the best tribo-mechanical performance, whereas CCPN resulted in superior surface finishing for application purposes.

**Keywords:** plasma-based nitriding; thermal diffusion; deposition; thin film; iron nitrides; S-phase



**Citation:** Schibicheski Kurelo, B.C.E.; De Souza, G.B.; Da Silva, S.L.R.; Lepienski, C.M.; Alves Júnior, C.; Chuproski, R.F.; Pintaúde, G. Tribo-Mechanical Behavior of Films and Modified Layers Produced by Cathodic Cage and Glow Discharge Plasma Nitriding Techniques. *Metals* **2023**, *13*, 430. <https://doi.org/10.3390/met13020430>

Academic Editors: Shinichiro Adachi, Francesca Borgioli and Thomas Lindner

Received: 30 January 2023

Revised: 14 February 2023

Accepted: 16 February 2023

Published: 19 February 2023



**Copyright:** © 2023 by the authors. Licensee MDPI, Basel, Switzerland. This article is an open access article distributed under the terms and conditions of the Creative Commons Attribution (CC BY) license (<https://creativecommons.org/licenses/by/4.0/>).

## 1. Introduction

Glow discharge plasma nitriding (GDPN) is a surface treatment widely used to improve the tribo-mechanical behavior of stainless-steels. Then, after the GDPN treatment, steel surfaces are expected to increase in hardness and wear resistance. Furthermore, depending on the microstructure of the formed layer, the corrosion resistance should be maintained or even improved after nitriding. Keeping the corrosion resistance at the same level as stainless-steel depends on the control of the formation of chromium and iron nitrides, by performing treatments at low temperatures and suitable times [1]. The modified layers are generally desirable to be rich in nitrogen-expanded austenite ( $\gamma_N$ ) phase, promoting excellent characteristics in stainless-steels [2,3].

There are some limitations associated with the use of GDPN treatment, such as the difficulty in treating samples with complex geometries, and the formation of non-uniform layers or edge effects. Both phenomena are associated with variations of the electric field around the sample in the plasma [4–6]. Furthermore, after GDPN treatments, surfaces undergo micrometric changes in the surface morphology due to sputtering/deposition and orientation-dependent anisotropic swelling. A relatively new technique that avoids these undesirable effects on the surface morphology is the cathodic cage plasma nitriding (CCPN) [5–8].

In the CCPN, a type of Physical Vapor Deposition (PVD) process, the sample is electrically isolated from the cathode and immersed in a floating electrical potential due to the presence of the surrounding and biased cathodic cage. Scientific evidence shows that a Kölbl's-like "sputtering and re-condensation" model, supposedly valid to the GDPN technique, is also applicable in a similar way to CCPN by considering the interaction among species from the atmosphere and adsorption on the surface [9]. In this process, electrons electrically trapped in the holes of the cage successively collide with atoms in the atmosphere, increasing the ion density. In this region, the ions, in turn, bombard the inner walls of the holes, sputtering atoms from the cage that will eventually be deposited on the surface of the sample. Thus, the plasma atmosphere, chemical composition of the cathodic cage, and arrangement of holes are parameters that govern the characteristics of the deposited film. In general, even carbon steel cages result in the deposition of iron nitrides on the electrically isolated substrates [5–7]. Another relevant feature of this technique is forming films that are brittle and thinner than the modified layers obtained by GDPN treatments, when employing the same treatment times [8,10]. However, the CCPN also allows the formation of a modified layer below the film due to nitrogen diffusion in the bulk, which is heated by thermal radiation. To our knowledge, it is not common to evaluate the modified diffusion layer formed below the film in CCPN treatments.

The wear performance of nitride layers depends on two aspects involving deformation. The first one is the level of the strain of the substrate, which can deform during contact between two bodies and correlates with hardness. Pintaude et al. [11] applied a method similar to CCPN, named active screen plasma nitriding (ASPN), for two duplex stainless-steels. They verified, after scratch tests, an occurrence of microcracks much more significant on the softer substrate than the harder one, featuring an eggshell effect. The other aspect is the relation between the load conditions and the layer thickness. For thicker nitrided layers processed onto martensitic stainless by ASPN, Rovani et al. [12] described less occurrence of cracks, as the thickness of the layers increased. In the same work, when the load in the scratch tests was reduced from 15 N to 8 N, cracks were not observed on the worn surfaces of the nitrided layers, emphasizing that the treated surfaces have a critical loading value that is important for the application of these layers [12]. These characteristics are important for films processed by CCPN and will be explored in the present study.

The surface mechanical strengthening of the AISI 316 stainless-steel finds applications in several areas, such as in biomedical devices, making it a good reason to investigate varied methods of nitriding for this alloy. Samanta et al. [13] carried out a detailed study of the mechanical and tribological behavior of nitrided AISI 316L surfaces, however they employed only one technique, the GDPN. Herein, the tribo-mechanical performance of 316 surfaces modified by GDPN, analyzed in micro/nanoscale, were contrasted with those subjected to CCPN. The study aims to contribute to the understanding of how the structure and microstructure of the layers affect the wear performance, as well as to the proper selection of the nitriding method.

## 2. Materials and Methods

Commercial samples of AISI 316 austenitic stainless-steel (15.7% Cr, 11.6% Ni, 1.7% Mn, 1.9% Mo, 0.3% Si, 0.1% C, 0.03% S, and 0.03% P, with Fe in balance) supplied by the company Villares Metals (São Paulo, SP, Brazil) were mechanically polished with sandpapers (SiC) and diamond pastes up to a 1  $\mu\text{m}$  particle size, and the final polishing

was carried out in a 15% volume solution of colloidal silica in  $\text{H}_2\text{O}_2$ . Before nitriding, the samples were cleaned with two ultrasound baths in acetone.

The equipment used for GDPN and CCPN is a custom-made equipment consisting of a vacuum chamber, an exhaust and a gas supply system, a voltage source, a K-type thermocouple and electronic sensors, described in detail in previous reports [6,14,15]. The treatment atmosphere was controlled by a flowmeter (model MKS 1179A, MKS Instruments, Andover, MA, USA), and the temperature by a thermocouple connected to the center of the sample holder (cathode). Voltage and current were monitored by a voltmeter and ammeter, both supplied by the company Minipa (São Paulo, SP, Brazil) and integrated into the voltage source. The chamber's internal pressure was measured by an Active Gauge controller RS 232 Edwards pressure gauge (Edwards Ltd., Burgess Hill, UK).

The samples were subjected to sputtering with  $\text{H}_2$  at  $(150 \pm 10)^\circ\text{C}$  and 300 Pa for one hour to remove the oxide surface layer and then nitrided by GDPN. An atmosphere of 1:4 ( $\text{N}_2:\text{H}_2$ ) (in volume), resulting in a total pressure of 300 Pa and a total flux of 20 sccm, was used. Both nitriding treatments by CCPN and GDPN were carried out at temperatures of  $350^\circ\text{C}$ ,  $400^\circ\text{C}$ , and  $450^\circ\text{C}$  for 6 h.

For CCPN treatments, a cathodic cage made of AISI 1008 steel was placed into the same GDPN equipment. Schematic diagrams for the GDPN and CCPN are shown in Figure 1. The material's chemical composition was 0.1% C, 0.5% Mn, 0.04% P, and 0.05% S (wt.%), in balance with Fe. The cage dimensions were  $112\text{ mm} \times 25\text{ mm} \times 0.8\text{ mm}$  (diameter  $\times$  height  $\times$  thickness), the diameter of the cage holes was 8 mm, and the distance between the center of adjacent holes was 9.2 mm. The samples were placed on an alumina insulator with a diameter of 55.8 mm. The cage was positioned above the cathode to enclose the alumina insulator assembly and the samples. The samples remained electrically isolated in this arrangement, and the cage was in electrical contact with the cathode. Initially, the cage was sputtered with  $\text{H}_2$  at  $200 \pm 5^\circ\text{C}$  for one hour at 30 Pa. After sputtering, the samples were nitrided by CCPN in an  $\text{N}_2:\text{H}_2$  atmosphere of 4:1 (in volume), resulting in a total pressure of the order of 80 Pa and an  $\text{N}_2/\text{H}_2$  gas flow of 16/4 sccm. These flow and pressure values in CCPN treatments were defined based on optimized sample properties in previous work [6,14,15]. The pressure value was defined as being the hollow cathode pressure the cage uses for that gaseous mixture, which is necessary to maximize the film thickness. The voltage varied between 464 V and 588 V during nitriding, according to the treatment temperature. A temperature of  $450^\circ\text{C}$  was chosen to evaluate the formation of chromium nitrides in the different techniques. The nitriding of AISI 316 steel for this work by GDPN and CCPN was carried out concomitantly with other martensitic steels, whose research was previously published [8,10].

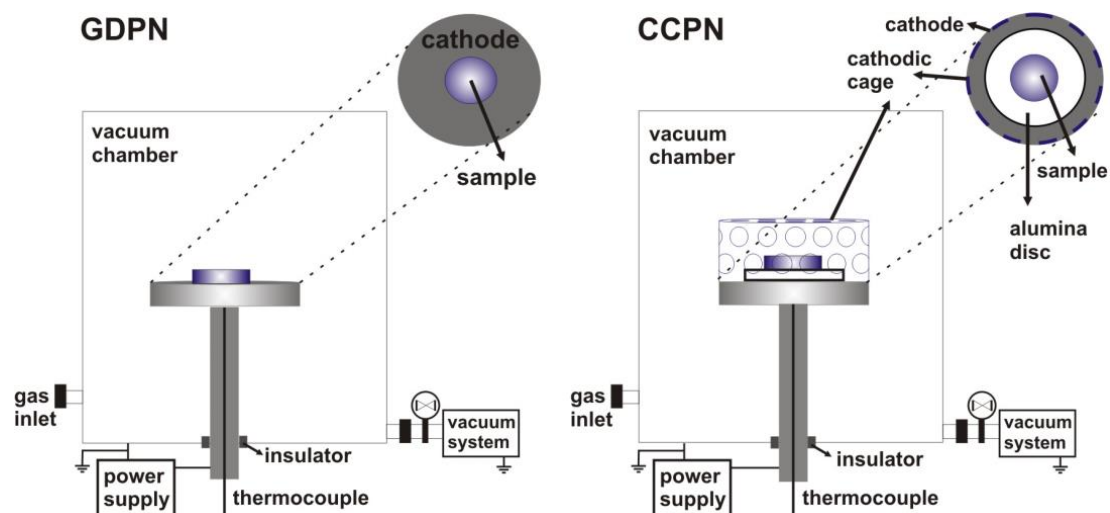


Figure 1. Schematic diagrams for the GDPN and CCPN treatments.

The cross-sections of the samples were mechanically polished and analyzed by field-emission gun scanning electron microscopy (FEG-SEM) model Mira3 (TESCAN, Koutovice, Czech Republic) equipped with energy dispersive spectroscopy (EDS) model XMaxN SDD (Oxford, Abingdon, UK) to evaluate the nitrogen uptake in the modified layers. Then, the chemical etching was carried out with Murakami's reagent composed by 10 g KOH and 10 g  $K_3Fe(CN)_6$  from the brand Sigma Aldrich (San Luis, MO, USA) and 50 ml  $H_2O$ , allowing the thickness of the modified layers to be measured through FEG-SEM analysis. In the samples treated by the CCPN technique, the thickness of the films was determined by optical interferometry (OI) model Talysurf CCI—Lite 3D (Taylor Hobson, Leicester, UK) on the surfaces of the samples, analyzing the height difference between the film surface and the interface with the modified layer in regions where the nitrides film was detached. OI estimated the roughness of all surfaces.

X-ray diffraction (XRD) data were collected by the X-ray diffractometer model Ultima IV (Rigaku, Tokyo, Japan.), with  $CuK\alpha$  radiation ( $\lambda = 0.15406$  nm), Bragg–Brentano geometry ( $\theta$ – $2\theta$ ), a  $0.02^\circ$  step, and a counting time of 4 s. The diffraction peaks were identified using powder crystallographic data sheets and literature data to  $\gamma_N$  phase peaks [3,16].

The nanoindentation technique was applied according to the ISO 14577-1 (2002) standard to measure the hardness and elastic modulus. The equipment used in the tests was an Nanoindenter XP (MTS Systems Corporation, Eden Prairie, MN, USA). Here, 25 indentations were performed with a Berkovich indenter arranged in a matrix with 100  $\mu m$  between the indentations. To obtain profiles of hardness and modulus of elasticity by depth, multiple-loading cyclic nanoindentation was used. The tests were carried out in the central regions of the samples with a maximum load of 400 mN and 8 loading–unloading cycles. For the analysis of the loading curves, the contact stiffness technique was used to minimize the roughness effect [17].

The nanoscratch tests were performed on the same equipment used in the nanoindentation tests. They were carried out with the Berkovich tip, with displacement towards one of the vertices, ramp loading (linear from zero), and a maximum load of 400 mN. The sliding speed was 10  $\mu m/s$ , and the scratch length was 600  $\mu m$ . The images of the nanoindentations and scratches were performed with a SEM model JSM-6360LV (JEOL, Peabody, MA, USA).

### 3. Results and Discussions

#### 3.1. Microstructural and Morphological Analysis

The microstructures of surfaces nitrified by GDPN and CCPN can be seen in Figure 2. All the surfaces were homogeneous after the treatment but, while the CCPN-nitrified surfaces showed small, sharp needle-shaped peaks, characteristic of the deposition process, the GDPN-treated samples disclosed broader peaks and valleys. For all the treatment conditions and at the same temperature, the difference in height between peaks and valleys was always smaller in the CCPN-nitrified surfaces when compared to GDPN-nitrified surfaces. This indicates that the mean roughness of samples treated by GDPN was always higher for the same treatment temperature and time.

Table 1 summarizes the thickness, roughness, and hardness (measured at a 200 nm depth) of layers and films produced by GDPN and CCPN techniques. The compared average roughness values were higher for all the GDPN conditions. Some possible explanations are plasma sputtering and swelling of grains, with the latter being more evident in GDPN than in CCPN. It is a result of the anisotropic retention of nitrogen in solid solution, dependent on the crystal direction of the grain, which is restrained laterally and grows toward the free surface [18]. The sputtering occurs via the non-uniform electric polarization of the sample in the plasma. According to accepted models [19], it plays an important role in the nitriding process since released atoms combine with ions from the plasma and fall with the ion flux toward the surface. This is likely a non-uniform process across the treated area and can result in the observed topography. On the contrary, average roughness values of the electrically isolated CCPN surfaces were similar to the reference one.

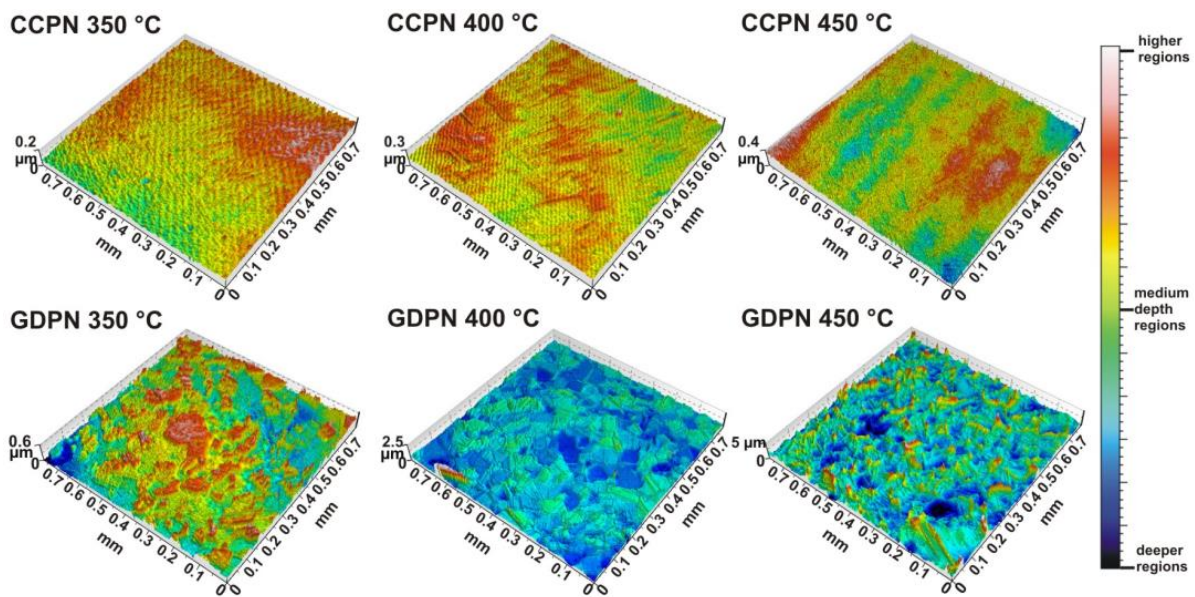


**Figure 2.** Surface microstructures of samples nitrided by CCPN and GDPN, obtained by OI.

**Table 1.** The thickness of modified layers and films, roughness, and hardness of the untreated and nitrided samples.

Sample	Layer Thickness Modified Layer ( $\mu\text{m}$ )	Layer Thickness Film ( $\mu\text{m}$ )	Roughness Ra (nm)	Roughness Rq (nm)	Top Hardness (GPa)
Untreated	-	-	$11.6 \pm 1.7$	$14.7 \pm 2.4$	$3.3 \pm 0.3$
GDPN 350 °C	$1.2 \pm 0.5$	-	$48.1 \pm 6.5$	$37.8 \pm 4.5$	$8.5 \pm 2.9$
GDPN 400 °C	$4.3 \pm 1.1$	-	$65.4 \pm 7.5$	$83.6 \pm 8.5$	$12 \pm 0.7$
GDPN 450 °C	$18.4 \pm 2.5$	-	$246.1 \pm 30.1$	$319.1 \pm 35.1$	$15.1 \pm 1.6$
CCPN 350 °C	$0.5 \pm 0.1$	$0.3 \pm 0.1$	$8.7 \pm 0.9$	$10.8 \pm 1$	$3.8 \pm 0.3$
CCPN 400 °C	$1.2 \pm 0.1$	$0.5 \pm 0.1$	$9.5 \pm 0.9$	$11.7 \pm 1.3$	$4.9 \pm 0.4$
CCPN 450 °C	$3.0 \pm 0.5$	$0.8 \pm 0.1$	$18.7 \pm 2.1$	$24.6 \pm 2.9$	$3.6 \pm 0.3$

Figure 3 shows the cross-section SEM images of surface plasma nitrided by GDPN and CCPN at the indicated temperatures, etched with Murakami's reagent. Modified layers are visible for all the nitriding treatments. At a same temperature, the thickness of the modified layer was smaller for the CCPN technique than for the GDPN technique. This difference increased with temperature, as seen in Table 1.

The nitrogen concentration shown in Figure 4 was obtained by EDS point analysis carried out in several points through the cross-section of the GDPN- and CCPN-treated samples. The N concentration was relatively higher for the GDPN technique than the CCPN one, for the same temperatures. In addition, the concentration profiles were consistent with the layer thicknesses, identified and measured after chemical etching, as seen in Figure 3 and summarized in Table 1.

In Figure 5, the nitride films produced by the CCPN technique were brittle and could be removed from the surface. The regions where the film was detached, such as the one shown in Figure 5a, were convenient to infer the film thickness, by measuring the height difference with the yN-rich surface below it. These height differences are presented in Figure 5b–d.

The average thickness of the films varied between  $0.3 \mu\text{m}$  and  $0.8 \mu\text{m}$  for CCPN 350 °C and CCPN 450 °C samples, respectively, as shown in Table 1. The values are close to those obtained by (Atomic Force Microscope) AFM in martensitic steels treated by the CCPN technique under the same conditions [8]. Thus, even by adding thicknesses of the nitride films with the modified layers produced by the CCPN technique, they were still thinner than those produced by the GDPN technique, in agreement with other studies [8,10,20]. On the other hand, standard deviations of films + layer thicknesses produced by CCPN were smaller, for all the treatment conditions, than the corresponding ones from the GDPN

technique. This result corroborates the homogeneity and uniformity of layers produced by the CCPN technique.

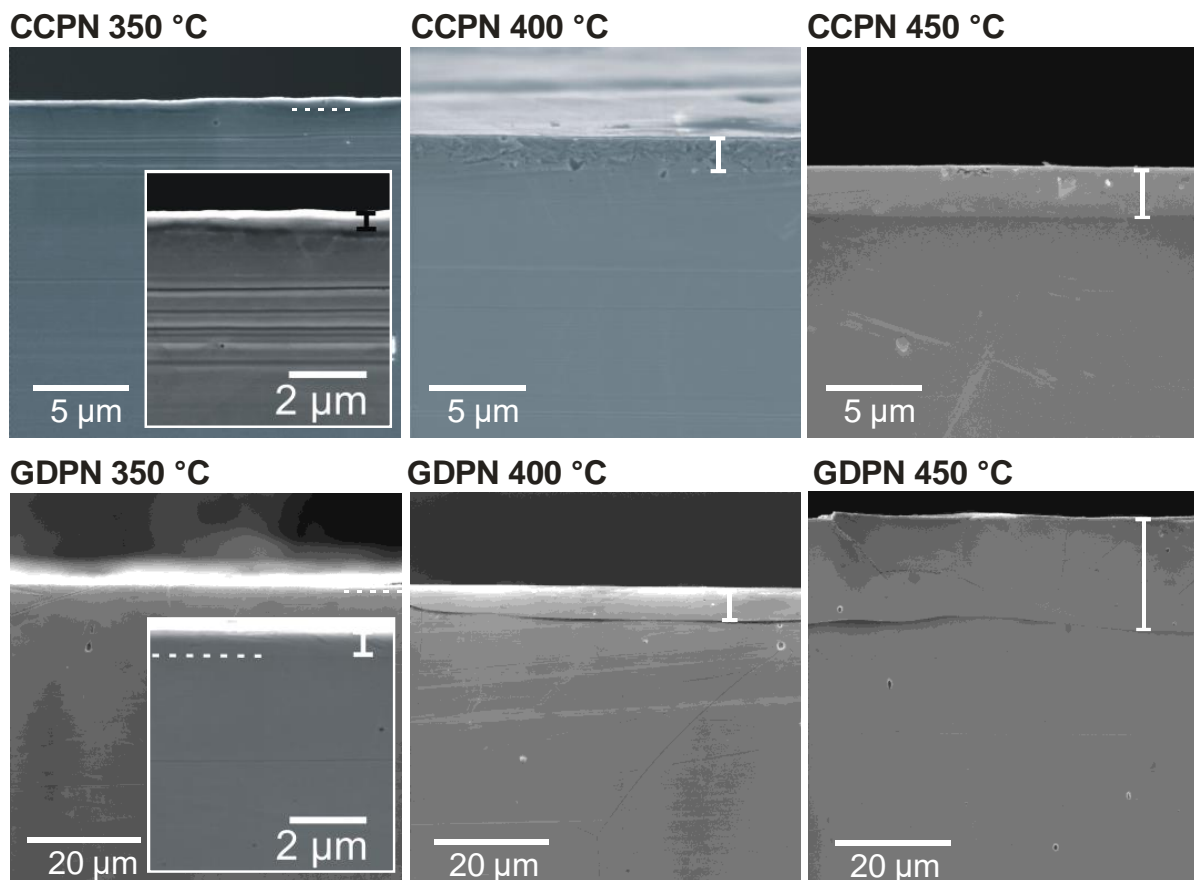


**Figure 3.** Cross-section SEM images of the plasma-nitrided samples by GDPN and CCPN at the indicated temperatures, etched with Murakami's reagent. Regions indicated correspond to modified layers produced, respectively.

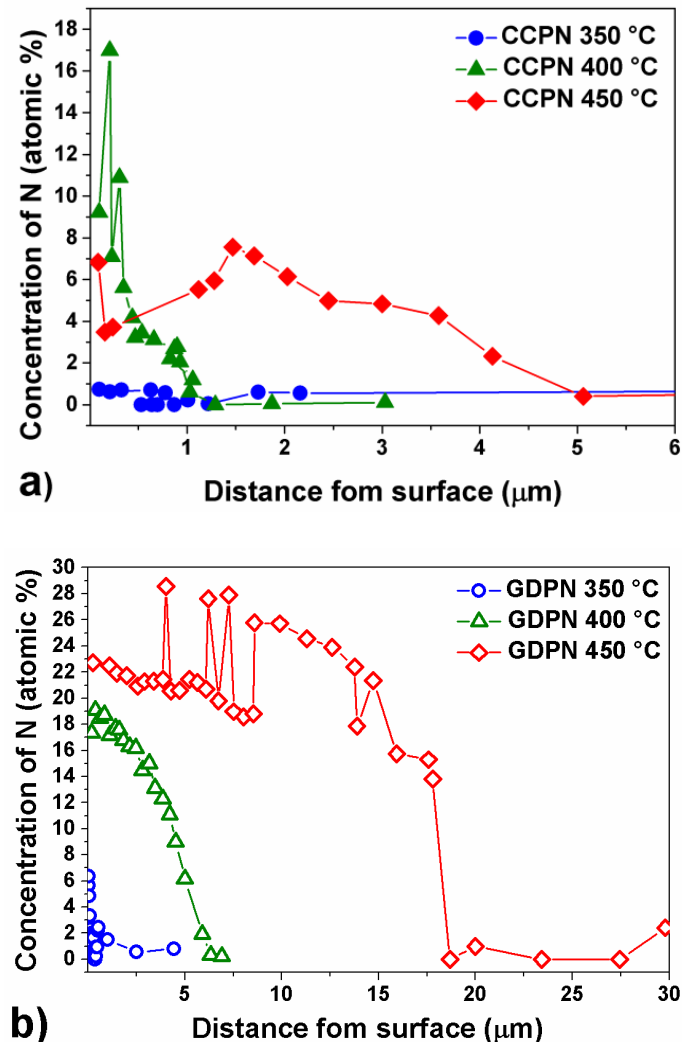
### 3.2. XRD Analysis

Figure 6 shows the X-ray diffractograms for the untreated sample and the samples nitrided by GDPN. The reference sample presented only the expected austenite peaks ( $\gamma$ ). After nitriding, the diffractogram of the GDPN 350 °C sample showed the nitrogen-expanded austenite ( $\gamma_N$  phase), which corresponded to the presence of nitrogen in solid solution in the steel's crystalline structure. The  $\gamma_N$  peak was wide, displaced to greater interplanar distances with regard to the  $\gamma$  phase. This phase corresponded to the superposition of several Fe(N) sub-stoichiometries of the nitrogen in solid solution, consisting in a gradient of lattice micro-strains.

In the sample GDPN 400 °C, the contribution of the  $\gamma$  phase peak considerably decreased compared to the GDPN 350 °C sample due to the increased thickness of the modified layer (Table 1). At this treatment temperature, the  $\gamma_N$  phase peak was displaced to greater interplanar distances, indicating a more significant expansion of the crystal lattice.

In the GDPN 450 °C sample, the diffractogram disclosed the formation of iron nitrides  $\gamma'$ -Fe<sub>4</sub>N and  $\epsilon$ -Fe<sub>2+x</sub>N (with  $x$  between 0 and 1), in addition to the drastic reduction of the peak's intensities corresponding to austenite. The formation of the  $\gamma'$  phase indicated that this temperature and treatment time were sufficient to cause the supersaturation of nitrogen in interstitial solid solution, resulting in the precipitation of nitrides [3]. After reaching the supersaturation limit, the formation of nitrides that have a lower enthalpy of formation occurred, such as the  $\gamma'$ -Fe<sub>4</sub>N phase. With increasing temperature, conditions became more favorable for the formation of nitrides that have a higher enthalpy of formation than

the  $\gamma'$  phase, i.e., the  $\varepsilon$  phase [21]. Then, with the increase in temperature from 400 °C to 450 °C, the replacement of  $\gamma_N$  by  $\gamma'$  and  $\varepsilon$  is expected. In addition, the increase of the temperature provided more favorable conditions for the diffusion of nitrogen into the steel. Thus, the increase in temperature led to forming a thicker modified layer with more precipitates [2,22,23].



**Figure 4.** The nitrogen concentration, in at.%, carried out in several points through the cross-section of the (a) GDPN- and (b) CCPN-treated samples.

At 450 °C, it was also possible to attribute contributions of the chromium nitride CrN in the diffractograms, a result of the chromium depletion in the steel [3]. This phenomenon is undesirable since the presence of Cr in the austenitic matrix is a determining factor for the “stainless” characteristic of the steel.

Figure 7 shows the diffractograms for the untreated and CCPN-nitrided samples. They significantly differed from the GDPN ones. Regardless of the treatment temperature, there was the formation of the  $\varepsilon$  phase. The analysis carried out from the crystallographic files revealed that this phase had predominantly the Fe<sub>2</sub>N stoichiometry. The  $\gamma'$ -Fe<sub>4</sub>N phase became more evident in the diffractogram corresponding to the 400 °C treatment. The expanded austenite phase ( $\gamma_N$ ) was also present in all treatment conditions but exhibiting smaller lattice expansions. The peak at  $\sim 43^\circ$  at temperatures of 350 °C and 400 °C and the peak at  $\sim 42.5^\circ$  in the sample nitrided at 450 °C were broad, as they have contributions from the  $\gamma$  and  $\gamma_N$  phases. The identified phases follow the literature results for this austenitic steel treated by CCPN [6,7,15]. In the CCPN process, the deposition phenomenon

prevails over diffusion, so iron nitride phases can be formed and deposited regardless of the treatment temperature.

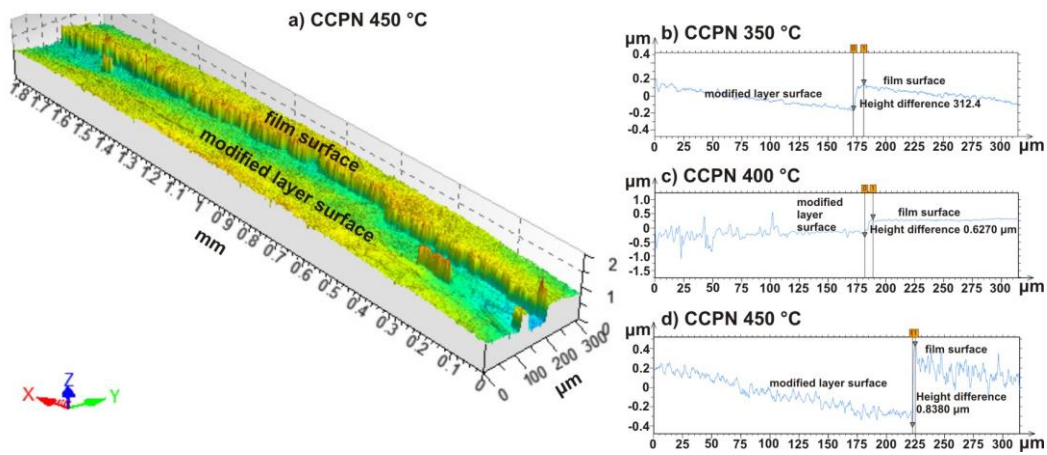


Figure 5. (a) Optical interferometry image of a region, on the CCPN 450 °C surface, showing the boundary between the nitride film and the hardened surface below it. (b–d) Analyses of the height differences between the film and modified layer surfaces.

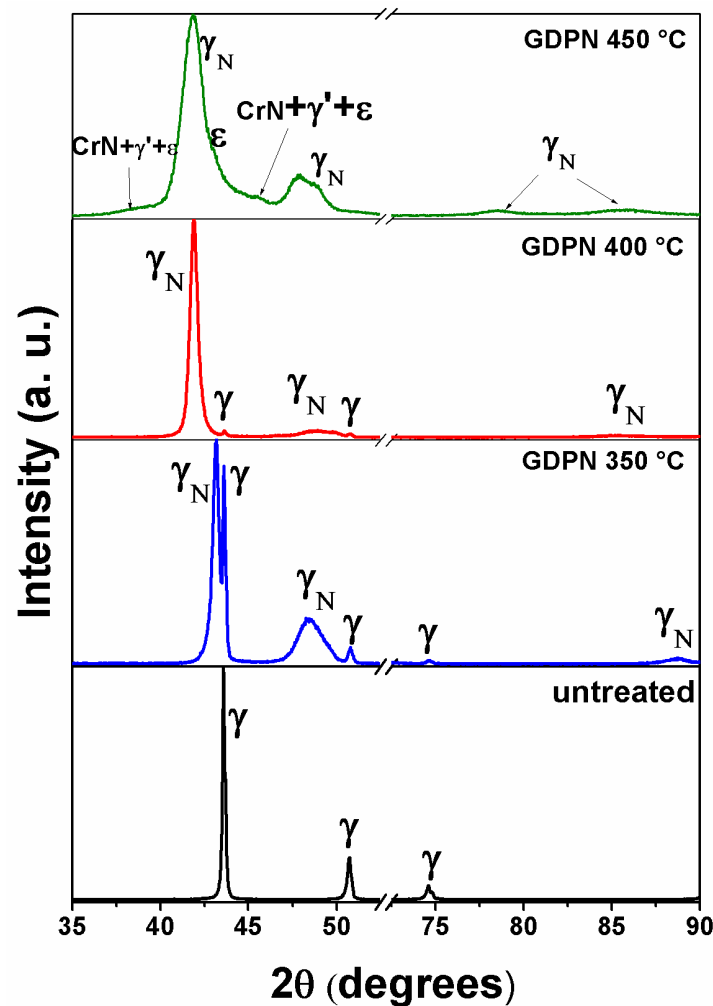
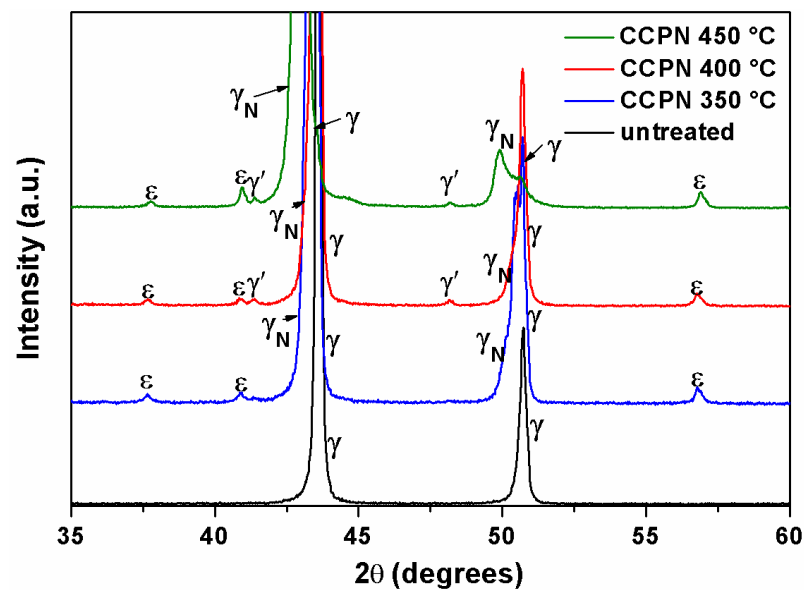
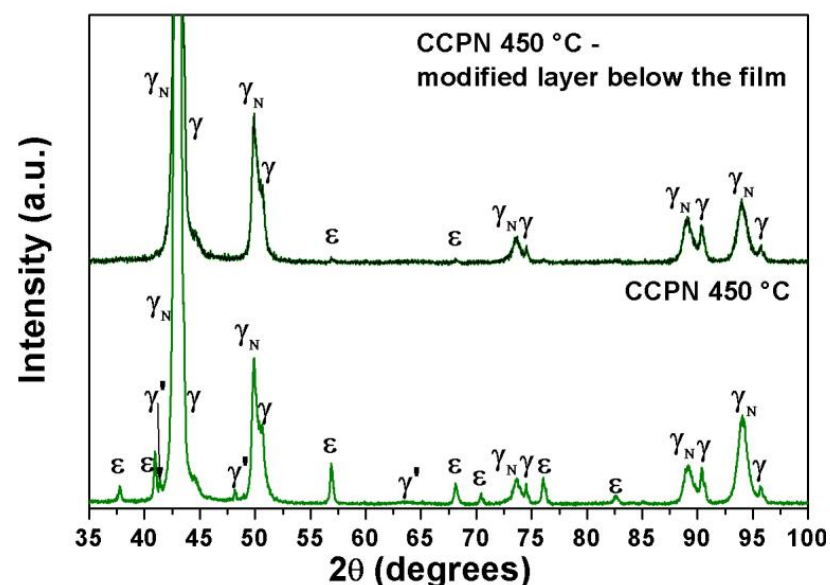


Figure 6. X-ray diffractograms for samples untreated and nitrided by GDPN AISI 316 steel at different temperatures.



**Figure 7.** X-ray diffractograms of samples untreated and nitrided by CCPN AISI 316 at different temperatures.

One advantage of the CCPN is a concomitant formation of a diffusion zone beneath the film. After removing the nitride layer from the GDPN 450 °C sample, the  $\gamma'$  phase was no longer identified in the diffractogram (Figure 8), while the predominant phase was  $\gamma_N$ . Hence, the N-solid solution laid mostly below the film, instead of composing it. The small  $\epsilon$  phase peaks in this diffractogram may be due to some layer residues that remained adhered to the surface. In the CCPN 450 °C sample, perhaps because the level of nitrogen supersaturation was low in the  $\gamma_N$  region below the film, it did not decay into  $\epsilon$ ,  $\gamma'$ , or chromium nitride phases. This result proves that a modified layer also formed below the film, despite the sample in the CCPN technique being electrically isolated from the cathode. Furthermore, after the formation of the film, it can act as a shield for the diffusion of nitrogen to the bulk. The diffusion of nitrogen into the matrix can be due to the release of N from unstable deposited phases, such as FeN [9].



**Figure 8.** X-ray diffractograms of the CCPN 450 °C sample for the nitrided layer and in the modified layer below the film deposited.

Comparing the techniques studied, GDPN and CCPN, it is relevant to stress that XRD did not identify chromium nitrides neither in the film nor in the modified layer produced by the CCPN technique. It can be attributed to the low nitrogen content in such coating. The absence of chromium nitrides is beneficial to preserve or increase the corrosion resistance of treated materials [24].

### 3.3. Nanoindentation Measurements

Figure 9 shows SEM micrographs of residual impressions produced by a Berkovich tip on the untreated and GDPN-nitrided AISI 316 steel samples. Lateral cracks were visualized in the GDPN 350 °C sample; however, none of the impressions disclosed radial cracks. The smaller residual impression on the GDPN 450 °C sample was a result of the high hardness of the layer. The surface morphology of the samples treated at 350 °C and 400 °C were similar to that of the untreated sample. In Figure 9d, the vertical structures around the indentation can be attributed to deformation twins.

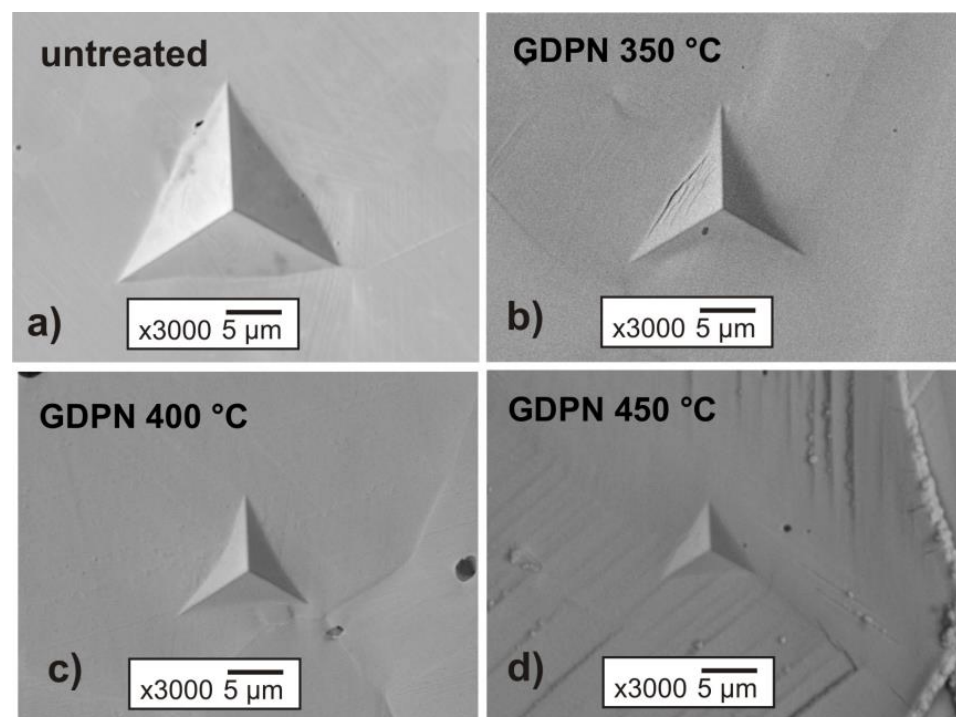
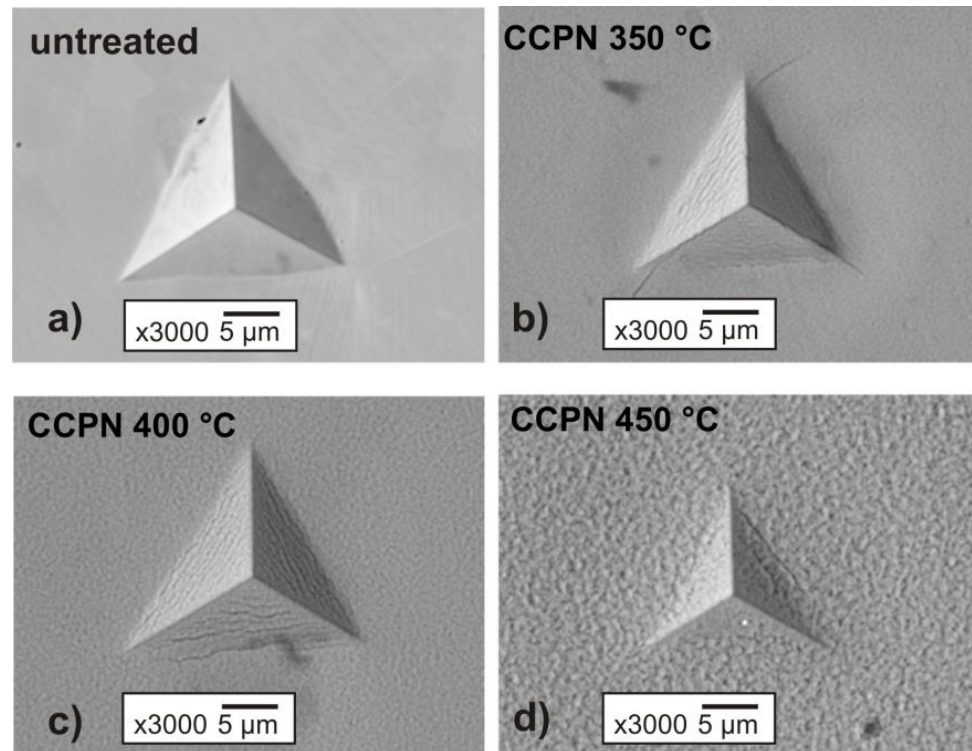


**Figure 9.** SEM micrographs of residual impressions produced by Berkovich tip indentation on untreated (a) and GDPN-nitrided (b–d) AISI 316 steel samples.

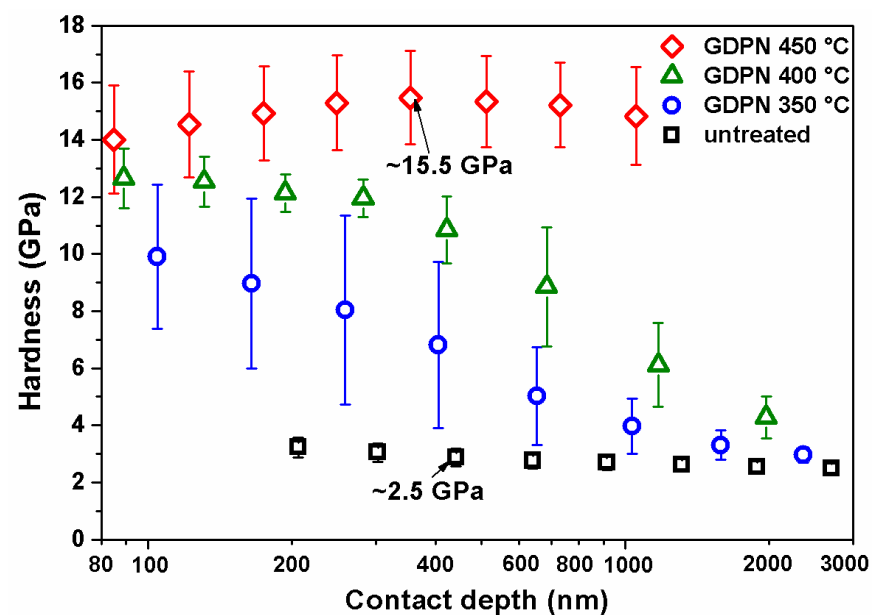
In CCPN treatments, however, the surface morphologies, shown in Figure 10, differed considerably from the original surface due to the film deposited on it, uniformly covering the surface. The residual impressions presented cracks for all the treatment temperatures, indicating the brittle behavior of these layers. The CCPN layer was not detached since the same surface morphology was also seen inside the indentation imprints. The residual impressions of the nitrided samples presented a reduction in the projected area compared to the impressions on the untreated sample, a conjoined result of the high hardness of CCPN layers and the nitrogen diffusion through the subsurface region (Figure 8).

Figure 11 shows hardness profiles of AISI 316 steel samples without treatment and treated by GDPN at different temperatures. The hardness profile of the reference sample was not constant due to the polishing-induced work hardening: it converged to  $2.5 \pm 0.2$  GPa. The GDPN 350 °C sample presented high hardness only on the top surface, decaying until reaching the substrate values at a depth of approximately 1100 nm, while the GDPN 400 °C sample had an initial “plateau”-shaped profile (values constant or within error bars) to approximately 280 nm, then decayed towards the substrate value. The hard-

ness profile for the GDPN 450 °C sample was approximately constant over the entire depth range analyzed, converging to  $15.2 \pm 1.5$  GPa at a depth of 730 nm. The large error bars for the 350 °C surface may, in addition to roughness effects, be due to the formation of lateral cracks (Figure 9) in the first stages of loading.



**Figure 10.** SEM micrographs of residual impressions produced by Berkovich tip indentation on untreated (a) and CCPN-nitrided (b–d) AISI 316 steel samples.



**Figure 11.** Hardness profiles of untreated and GDPN-nitrided samples.

The hardness profiles agreed with the X-ray diffractograms of these samples (Figure 6). In the samples treated at 350 °C and 400 °C, due to the predominant formation of the  $\gamma_N$  phase, the primary hardening mechanism was solid solution formation, in which interstitial atoms can migrate to sites in the dislocations. This phenomenon, known as

the “Cottrell atmosphere,” prevents the movement of dislocations and can reduce the number of slip systems, increasing the material’s resistance to plastic deformation. The GDPN 450 °C sample may also present the precipitation hardening and dispersion as a contributing mechanism due to the formation of  $\epsilon$  and  $\gamma'$  precipitates that act as obstacles to the movement of dislocations, increasing the material’s resistance to plastic deformation.

The graph in Figure 12a shows hardness profiles of the untreated and CCPN-nitrided AISI 316 steel surfaces. The behavior of the 350 °C and 450 °C conditions was similar to the untreated one at depths below ~200 nm. The sample treated at 400 °C showed an increase in hardness profiles from  $3.3 \pm 0.3$  GPa to  $5.5 \pm 0.5$  GPa. However, the CCPN 450 °C curve presented an elevation at shallow depths and then a decrease after ~600 nm. This phenomenon may be related to the intense brittleness of the layer produced by CCPN when it is subjected to normal loading, as it can be seen in the indentation imprints shown in Figure 10. The imprints disclosed radial or lateral cracks, which caused errors in the calculated hardness values. In addition, all hardness profiles of the nitrided samples converged to substrate values (untreated sample) at a ~2600 nm depth.

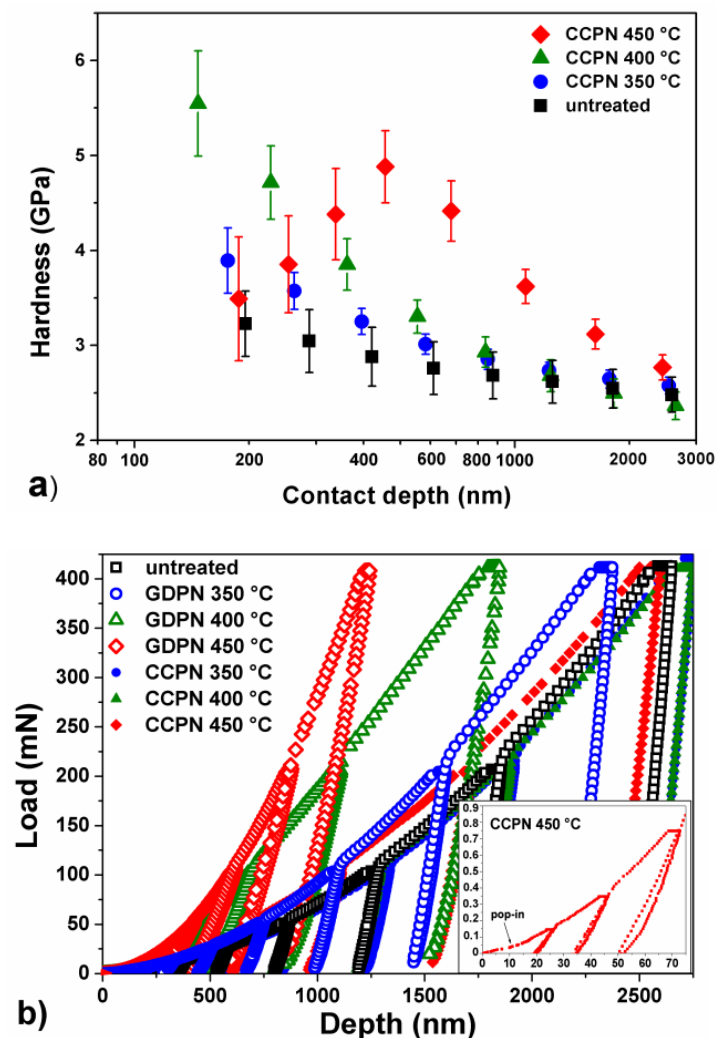


**Figure 12.** (a) Hardness profiles of untreated and CCPN-nitrided samples and (b) loading curves for all samples. The inset shows a pop-in event in the loading curve of the CCPN 450 °C sample.

In Figure 12b, loading curves for all samples are presented. Analyzing the loading curves of the sample treated at 450 °C (Figure 12b), it is observed that a significant change in inclination and a pop-in occurred in the first stages of loading which, in this case, can be attributed to the formation of fractures. The film yielded under the indenter, causing incursions into the material without the need of increasing the applied load. Consequently,

the algorithm of the equipment underestimated the hardness values obtained by the Oliver and Pharr method (in which  $H \propto 1/h_c^2$ ) [25].

Figure 13 shows the hardness profile obtained after the removal of the film from the CCPN 450 °C sample surface, which revealed a nitrogen diffusion zone, as identified by XRD (Figure 8). The hardness profile no longer presented the anomalous behavior shown in Figure 12a while disclosing a GDPN-like behavior (Figure 11) at this modified layer. The hardness at a depth of ~200 nm was  $9.2 \pm 0.7$  GPa, that is, greater than that ( $3.6 \pm 0.3$  GPa) for the nitride film over the same sample. It was also of the same order of values, reported by others, for cross-sectional profiles measured in the same AISI 316 and AISI316L treated by CCPN [6,26]; probably, with the microhardness method, they could not test the thin nitride layer separately. The hardness obtained for the CCPN 450 °C condition, below the nitride film, was lower than that measured on surfaces treated by GDPN at the same temperature, in agreement with other works [8,10,20,26,27]. Moreover, the hardness values were very close to those obtained for the GDPN 350 °C condition (Figure 11), where  $\gamma_N$  was the main phase (Figure 6). In the absence of a plateau in the profiles and considering the 10% rule [28], we can estimate that this modified layer had a thickness of ~1  $\mu\text{m}$ . As already mentioned, the origin of this nitrogen diffusion zone in samples electrically isolated in the plasma chamber may be related to the deposition and subsequent dissociation of unstable nitride species (FeN) and their diffusion by thermal effects [9,29].

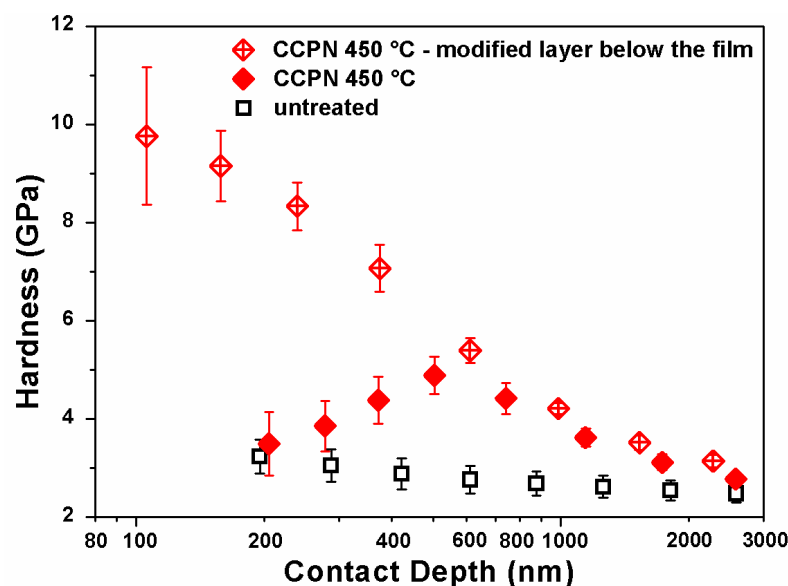


**Figure 13.** Hardness profiles of the CCPN 450 °C sample in the film and the region below the deposited film compared to the untreated sample.

These results suggest that the anomalous and low hardness profiles (compared to GDPN treatments under similar conditions) shown in Figure 12a are related to the brittle nitride layer produced by the cathodic cage. The true hardness of the layer can even be high, in the order of values observed for conventional plasma treatments, since it is made up of iron nitrides (Figure 7). However, the generation of cracks prevents the correct determination of hardness by normal loading indentation.

### 3.4. Scratch Tests

Figure 14 presents profiles obtained during and after scratching of untreated and GDPN-nitrided surfaces, with micrographs from central regions of the grooves.

The maximum depth and elastic recovery values are summarized in Table 2. The penetration depth profiles during loading, the residual depth of the nanoscratch tracks, and the track widths were smaller in the nitrided samples than in the reference sample (not shown). These characteristics agree with the mechanical strengthening of the surfaces,

which increased with treatment temperatures. On the surface nitrided at 450 °C, the morphology influenced the nanoscratch path so that the tip course deviated near structures that can be swelled grain boundaries. On this surface, a step-like topography in the inner region of the track can also be observed, which is reflected in the “rough” aspect of the scratch profile. In all the nitrided samples, the elastic recovery of the surface after the load removal was more significant than in the untreated condition. The maximum scratch depth in samples treated at 400 °C and 450 °C was within the range evaluated for layer thicknesses ( $\geq 3.2 \mu\text{m}$ ). However, the overall behavior of the scratch profiles did not significantly differ from the untreated sample, despite the ~4-fold increase in hardness. This fact may be associated with the abrasive action of hard nitride precipitates that were removed and displaced by the tangential movement of the tip. The samples GDPN 350 °C and GDPN 450 °C had elastic recovery close to those of the reference sample, and the sample GDPN 400 °C had a maximum scratch penetration depth of approximately half the value of the untreated sample.

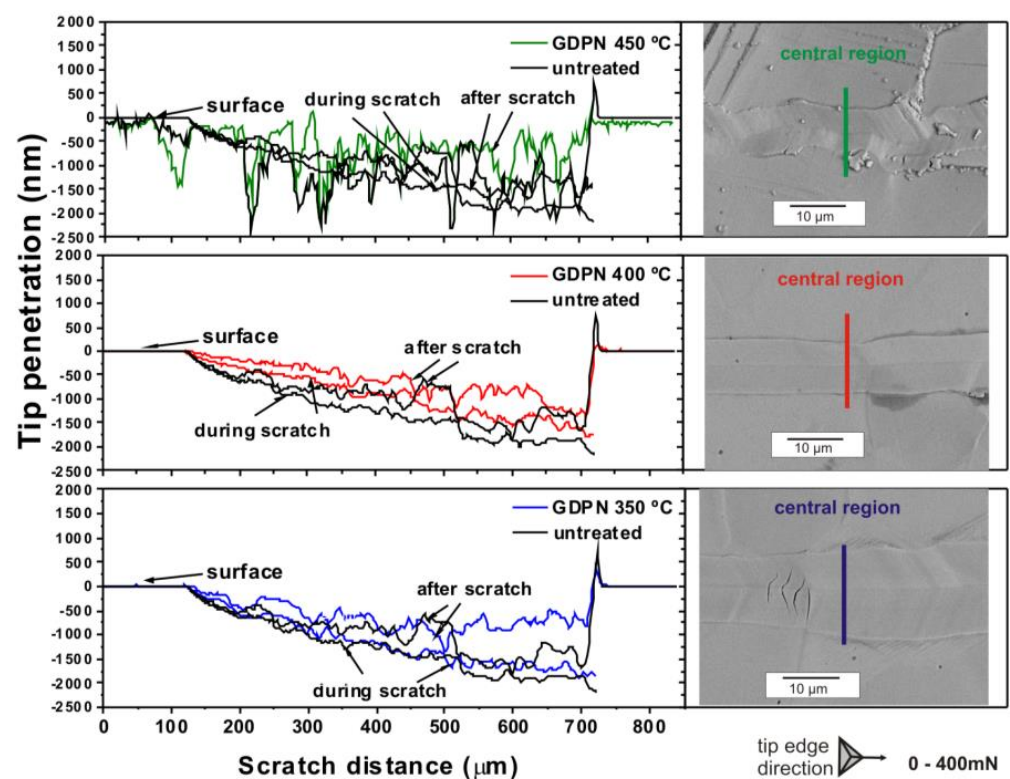


**Figure 14.** Nanoscratch profiles of untreated and GDPN-treated AISI 316 steel samples and micrographs obtained by backscattered SEM.

**Table 2.** Critical load, maximum depth, and elastic recovery (under 200 mN load) of untreated and nitrided samples.

Sample	Critical Load (mN)	Maximum Depth (nm)	Elastic Recovery (%)
Untreated	-	1375 ± 64	22 ± 8
GDPN 350 °C	-	1281 ± 66	33 ± 5
GDPN 400 °C	-	698 ± 67	55 ± 6
GDPN 450 °C	-	1254 ± 35	35 ± 3
CCPN 350 °C	9 ± 1	1434 ± 39	-
CCPN 400 °C	63 ± 13	1225 ± 24	-
CCPN 450 °C	24 ± 2	1575 ± 22	-

Figure 15 shows electron micrographs of the scratch path produced on the untreated and CCPN-treated samples. It is possible to observe regions where the film was delaminated

and fractured, while in the rest of the track the scratching caused fragmentation and detachment of the nitride layer.

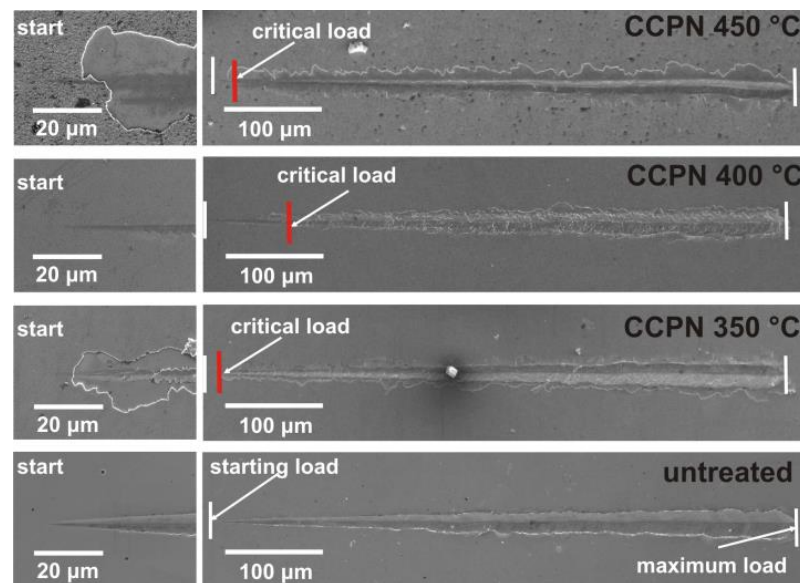


**Figure 15.** Nanoscratch micrographs of untreated and CCPN-treated AISI 316 steel samples obtained by SEM.

The critical load of scratching at which the film remained adhered to the substrate can be taken as a comparison measurement of the performance among the different CCPN surfaces. Figure 16 shows the profile graph and nanoscratch micrograph of the AISI 316 steel sample treated at 400 °C for 6 h. In Figure 16, in the backscattered SEM image, it is possible to identify by contrast (due to the different chemical compositions) the nitride film and regions where it was chipped. Therefore, the lighter region corresponds to the substrate exposed after removing the nitride film (the darker region). The distance from which the film chipping occurred was approximately 112 µm from the scratch beginning. At this distance, the penetration curve changed in slope and roughness during loading; from this position on, the removal of the film became more pronounced. The critical load for scratch resistance at this point was 63 mN. With this methodology, we obtained the critical load values for the scratch resistance of the CCPN-nitrided surfaces, which are summarized in Table 2. Among the treatments with a cathode cage, the CCPN 400 °C sample showed the highest critical load value for scratch resistance, with a mean value of  $(63 \pm 13)$  mN. A similar behavior was observed in treatments performed on martensitic steels nitrided under the same conditions [8].

Steels that undergo nitriding processes are typically employed under severe wear and abrasion conditions. Therefore, the film deposited for these applications should withstand loads higher than those used in this test ( $400 \text{ mN} = 40 \text{ gf}$ ); however, the maximum critical load of the formed films was only  $\sim 63 \text{ mN}$ . In practice, this brittle and nitride-rich film can act as a sacrificial layer, where wear and corrosion simultaneously occur. In addition, according to the literature, the CCPN treatments can enhance the corrosion resistance of austenitic steels [30]. After the rupture of this top layer, a modified and homogeneous surface where  $\gamma_N$  is the predominant phase will be exposed to the working conditions. It is expected that in this condition, the sample will show good tribological performance associated with good corrosion resistance. Therefore, additional tribological and corrosion resistance studies are necessary to evaluate if the nitrides and  $\gamma_N$  layer may act together as a complex system.

Regarding the maximum depths, the lowest value was observed for the GDPN 400 °C sample. In this situation, there was a  $\sim 50\%$  reduction in the maximum depth compared to the untreated sample. In contrast, the maximum depth reached by the CCPN-treated

samples was very close to or higher than that of the untreated sample, possibly due to film breakage and incorporation of debris in the abrasion process within the wear track.

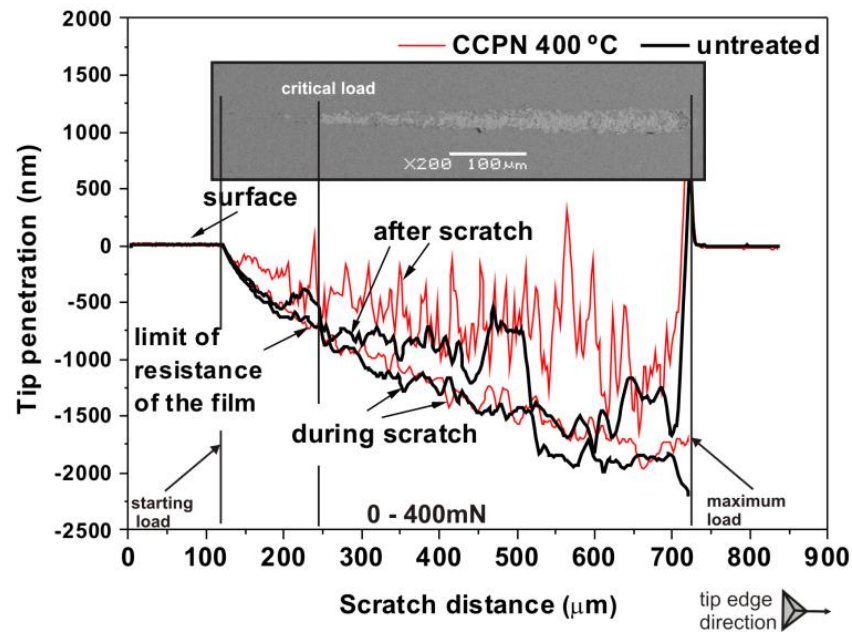


**Figure 16.** Profile graph and nanoscratch micrograph obtained by backscattered SEM of the AISI 316 steel sample treated at 400 °C for 6 h by CCPN.

Figure 17 presents the cross-section topographies of grooves produced on surfaces nitrided at 400 °C by CCPN and GDPN, which were the ones that presented the best tribological performance in each of the nitriding techniques.

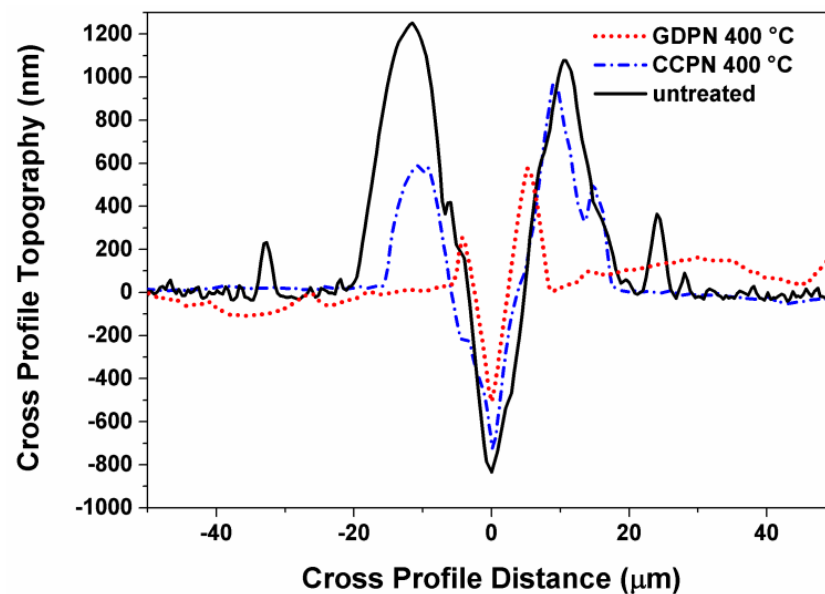


**Figure 17.** Cross-section topographies taken at the grooves' middle regions, corresponding to 200 mN of applied load.

In agreement with the previous analyses, the grooves' profiles of the GDPN 400 °C surface were consistent with the best wear resistance, as evidenced by the reduction in the residual depth (analyzed after removing the load) and a considerably lower pile-up.

#### 4. General Remarks

To sum up, the results obtained for the GDPN 400 °C sample were superior to those obtained for the samples treated by CCPN, and they also corroborated the best performance of this GDPN treatment, among the conditions studied here, for improving the tribological behavior of the AISI 316L steel at typical applications.

On the other hand, below a brittle thin layer, the CCPN resulted in graded  $\gamma_N$ -rich cases, which were also well-established with the substrate and (an important feature) free from the undesirable edge effect. A possible solution to achieve the best of both processes, avoiding the brittleness of nitride films, is to keep the material under treatment in the cathodic cage but electrically biased, instead of in a floating potential. This condition is expected to prioritize the formation of the modified layer to the detriment of the film deposition process, therefore reducing the edge effect. Some researchers have reported good results in this treatment condition [31], which is planned to be investigated by nanoindentation and nanoscratch in the future.

#### 5. Conclusions

At temperatures between 350 °C and 450 °C, the surface modification by CCPN produced 0.3–0.8  $\mu\text{m}$ -thick nitride films with low roughness ( $8.7 \text{ nm} < \text{Ra} < 18.7 \text{ nm}$ ), laying above and presenting a well-defined interface with a 0.5–3  $\mu\text{m}$ -thick nitrogen solid solution ( $\gamma_N$ ) region. The GDPN treatments produced thicker modified layers (1.2–18  $\mu\text{m}$ ), composed of  $\gamma_N$  phase and nitrides, with higher roughness ( $48 \text{ nm} < \text{Ra} < 246 \text{ nm}$ ) than CCPN.

In the GDPN technique, different phases ( $\gamma_N$ ,  $\gamma'$ -Fe<sub>4</sub>N,  $\epsilon$ -Fe<sub>2+x</sub>N, CrN) were formed with a predominance of the  $\gamma_N$  phase in treatments carried out at low temperatures (up to 400 °C). In the CCPN treatments, the formation of the  $\epsilon$  phase occurred independently of the treatment temperature due to the deposition process. High temperatures (from 450 °C) in CCPN treatments favored the formation of a modified layer rich in  $\gamma_N$  phase below the film due to the greater diffusion of nitrogen to the substrate; however, chromium nitrides were absent from both layers, which is an interesting feature for the corrosion resistance.

The GDPN 450 °C sample presented the highest hardness values (15.5 GPa) among the studied conditions, while in the CCPN 450 °C sample, below the brittle nitrides layer, hardness was 10 GPa, 35% smaller than the GDPN 450 °C sample.

The scratch resistance of the GDPN-nitrided surfaces significantly increased as compared to the untreated sample. The film from the CCPN-treated samples showed less scratch resistance due to delamination and cracking of the films during the analyses. The highest critical load for scratch resistance was  $63 \pm 13 \text{ mN}$ .

The layers produced by the GDPN technique were more mechanical-resistant than those produced by the CCPN technique. However, depending on the application, the corrosion resistance of these layers must be evaluated. In addition, due to uniformity, low roughness, and absence of chromium depletion, surfaces modified by CCPN may perform better than the ones subjected to the GDPN technique, providing that the top brittle nitride layer can be removed or is irrelevant for application purposes.

**Author Contributions:** Conceptualization, B.C.E.S.K., G.B.D.S. and S.L.R.D.S.; methodology, B.C.E.S.K., G.B.D.S. and S.L.R.D.S.; formal analysis, B.C.E.S.K., G.B.D.S., S.L.R.D.S., C.M.L., C.A.J., R.F.C. and G.P.; investigation, B.C.E.S.K. and R.F.C.; data curation, B.C.E.S.K.; writing—original draft preparation, B.C.E.S.K.; writing—review and editing, G.B.D.S., S.L.R.D.S., C.M.L., C.A.J., R.F.C. and G.P. All authors have read and agreed to the published version of the manuscript.

**Funding:** Bruna Kurelo was supported by a postdoctoral research scholarship PNPd granted by the Coordination for the Improvement of Higher Education Personnel during the completion of this research.

**Institutional Review Board Statement:** Not applicable.

**Informed Consent Statement:** Not applicable.

**Data Availability Statement:** The data used in this research are available in the article.

**Acknowledgments:** The authors thank the C-LABMU/UEPG, CCM/UTFPR, LabNano/UFPR and CME/UFPR for the use of characterization facilities.

**Conflicts of Interest:** The authors declare no conflict of interest.

## References

1. Olzon-Dionysio, M.; de Souza, S.D.; Basso, R.L.O.; de Souza, S. Application of Mössbauer Spectroscopy to the Study of Corrosion Resistance in NaCl Solution of Plasma Nitrided AISI 316L Stainless Steel. *Surf. Coat. Technol.* **2008**, *202*, 3607–3614. [[CrossRef](#)]
2. Nascimento, F.C.; Foerster, C.E.; Da Silva, S.L.R.; Lepienski, C.M.; Siqueira, C.J.D.M.; Junior, C.A. A Comparative Study of Mechanical and Tribological Properties of AISI-304 and AISI-316 Submitted to Glow Discharge Nitriding. *Mater. Res.* **2009**, *12*, 173–180. [[CrossRef](#)]
3. Dong, H. S-Phase Surface Engineering of Fe-Cr, Co-Cr and Ni-Cr Alloys. *Int. Mater. Rev.* **2010**, *55*, 65–98. [[CrossRef](#)]
4. Olzon-Dionysio, M.; Campos, M.; Kapp, M.; de Souza, S.; de Souza, S.D. Influences of Plasma Nitriding Edge Effect on Properties of 316L Stainless Steel. *Surf. Coat. Technol.* **2010**, *204*, 3623–3628. [[CrossRef](#)]
5. Junior, C.A.; Freitas, N.V.D.S.; De Moraes, P.B.; Vitoriano, J.D.O. Changing the Characteristics of the Nitrided Layer Using Three Different Plasma Configurations. *Rev. Mater.* **2019**, *24*, 1–8. [[CrossRef](#)]
6. De Sousa, R.R.M.; De Araújo, F.O.; Gontijo, L.C.; Da Costa, J.A.P.; Alves, C. Cathodic Cage Plasma Nitriding (CCPN) of Austenitic Stainless Steel (AISI 316): Influence of the Different Ratios of the (N<sub>2</sub>/H<sub>2</sub>) on the Nitrided Layers Properties. *Vacuum* **2012**, *86*, 2048–2053. [[CrossRef](#)]
7. Alves, C.; de Araújo, F.O.; Ribeiro, K.J.B.; da Costa, J.A.P.; Sousa, R.R.M.; de Sousa, R.S. Use of Cathodic Cage in Plasma Nitriding. *Surf. Coat. Technol.* **2006**, *201*, 2450–2454. [[CrossRef](#)]
8. Kurelo, B.C.; de Souza, G.B.; da Silva, S.L.R.; Daudt, N.D.F.; Alves, C.; Torres, R.D.; Serbena, F.C. Tribo-Mechanical Features of Nitride Coatings and Diffusion Layers Produced by Cathodic Cage Technique on Martensitic and Supermartensitic Stainless Steels. *Surf. Coat. Technol.* **2015**, *275*, 41–50. [[CrossRef](#)]
9. Saeed, A.; Khan, A.W.; Jan, F.; Abrar, M.; Khalid, M.; Zakaullah, M. Validity of “Sputtering and Re-Condensation” Model in Active Screen Cage Plasma Nitriding Process. *Appl. Surf. Sci.* **2013**, *273*, 173–178. [[CrossRef](#)]
10. Kurelo, B.C.E.S.; De Souza, G.B.; Da Silva, S.L.R.; Serbena, F.C.; Foerster, C.E.; Alves, C. Plasma Nitriding of HP13Cr Supermartensitic Stainless Steel. *Appl. Surf. Sci.* **2015**, *349*, 403–414. [[CrossRef](#)]
11. Pintaude, G.; Rovani, A.C.; das Neves, J.C.K.; Lagoeiro, L.E.; Li, X.; Dong, H.S. Wear and Corrosion Resistances of Active Screen Plasma-Nitrided Duplex Stainless Steels. *J. Mater. Eng. Perform.* **2019**, *28*, 3673–3682. [[CrossRef](#)]
12. Rovani, A.C.; Breganon, R.; de Souza, G.S.; Brunatto, S.F.; Pintaude, G. Scratch Resistance of Low-Temperature Plasma Nitrided and Carburized Martensitic Stainless Steel. *Wear* **2017**, *376–377*, 70–76. [[CrossRef](#)]
13. Samanta, A.; Chakraborty, H.; Bhattacharya, M.; Ghosh, J.; Sreemany, M.; Bysakh, S.; Rane, R.; Joseph, A.; Jhala, G.; Mukherjee, S.; et al. Nanotribological Response of a Plasma Nitrided Bio-Steel. *J. Mech. Behav. Biomed. Mater.* **2017**, *65*, 584–599. [[CrossRef](#)] [[PubMed](#)]
14. de Sousa, R.R.M.; de Araújo, F.O.; da Costa, J.A.P.; Brandim, A.D.S.; de Brito, R.A.; Alves, C. Cathodic Cage Plasma Nitriding: An Innovative Technique. *J. Metall.* **2012**, *2012*, 1–6. [[CrossRef](#)]
15. de Sousa, R.R.M.; de Araújo, F.O.; Gontijo, L.C.; da Costa, J.A.P.; Nascimento, I.O.; Alves, C., Jr. Cathodic Cage Plasma Nitriding of Austenitic Stainless Steel (AISI 316): Influence of the Working Pressure on the Nitrided Layers Properties. *Mater. Res.* **2014**, *17*, 427–433. [[CrossRef](#)]
16. Manova, D.; Mändl, S.; Neumann, H.; Rauschenbach, B. Formation of Metastable Diffusion Layers in Cr-Containing Iron, Cobalt and Nickel Alloys after Nitrogen Insertion. *Surf. Coat. Technol.* **2017**, *312*, 81–90. [[CrossRef](#)]
17. Souza, G.; Foerster, C.; Silva, S.; Lipienski, C. Nanomechanical Properties of Rough Surfaces. *Mater. Res.* **2006**, *9*, 159–163. [[CrossRef](#)]
18. Oliveira, W.; Kurelo, B.C.E.S.; Ditzel, D.G.; Foerster, C.E.; Serbena, F.C.; de Souza, G.B. On the S-Phase Formation and the Balanced Plasma Nitriding of Austenitic-Ferritic Super Duplex Stainless Steel. *Appl. Surf. Sci.* **2018**, *434*, 1161–1174. [[CrossRef](#)]
19. Pastukh, I.M. Energy Model of Glow Discharge Nitriding. *Tech. Phys.* **2016**, *61*, 76–83. [[CrossRef](#)]
20. Kovács, D.; Quintana, I.; Dobránszky, J. Effects of Different Variants of Plasma Nitriding on the Properties of the Nitrided Layer. *J. Mater. Eng. Perform.* **2019**, *28*, 5485–5493. [[CrossRef](#)]
21. Tessier, F.; Navrotsky, A.; Niewa, R.; Leineweber, A.; Jacobs, H.; Kikkawa, S.; Takahashi, M.; Kanamaru, F.; DiSalvo, F.J. Energetics of Binary Iron Nitrides. *Solid State Sci.* **2000**, *2*, 457–462. [[CrossRef](#)]
22. Nascimento, F.C.; Lepienski, C.M.; Foerster, C.E.; Assmann, A.; Da Silva, S.L.R.; Siqueira, C.J.D.M.; Chinelatto, A. Structural, Mechanical, and Tribological Properties of AISI 304 and AISI 316L Steels Submitted to Nitrogen-Carbon Glow Discharge. *J. Mater. Sci.* **2009**, *44*, 1045–1053. [[CrossRef](#)]
23. Lepienski, C.; Nascimento, F.; Foerster, C.; da Silva, S.; Siqueira, C.D.M.; Alves, C. Glow Discharge Nitriding in AISI 304 at Different Nitrogen-Hydrogen Atmospheres: Structural, Mechanical and Tribological Properties. *Mater. Sci. Eng. A* **2008**, *489*, 201–206. [[CrossRef](#)]
24. Chiu, L.H.; Su, Y.Y.; Chen, F.S.; Chang, H. Microstructure and Properties of Active Screen Plasma Nitrided Duplex Stainless Steel. *Mater. Manuf. Process.* **2010**, *25*, 316–323. [[CrossRef](#)]

25. Oliver, W.C.; Pharr, G.M. An Improved Technique for Determining Hardness and Elastic Modulus Using Load and Displacement Sensing Indentation Experiments. *J. Mater. Res.* **1992**, *7*, 1564–1583. [[CrossRef](#)]
26. Borowski, T.; Adamczyk-Cieślak, B.; Brojanowska, A.; Kulikowski, K.; Wierzchoń, T. Surface Modification of Austenitic Steel by Various Glow-Discharge Nitriding Methods. *Mater. Sci.* **2015**, *21*, 376–381. [[CrossRef](#)]
27. Sumiya, K.; Tokuyama, S.; Nishimoto, A.; Fukui, J.; Nishiyama, A. Application of Active-Screen Plasma Nitriding to an Austenitic Stainless Steel Small-Diameter Thin Pipe. *Metals* **2021**, *11*, 366. [[CrossRef](#)]
28. Saha, R.; Nix, W.D. Effects of the Substrate on the Determination of Thin Film Mechanical Properties by Nanoindentation. *Acta Mater.* **2002**, *50*, 23–38. [[CrossRef](#)]
29. Fraczek, T.; Prusak, R.; Ogórek, M.; Skuza, Z. Nitriding of 316L Steel in a Glow Discharge Plasma. *Materials* **2022**, *15*, 3081. [[CrossRef](#)]
30. Borowski, T. Enhancing the Corrosion Resistance of Austenitic Steel Using Active Screen Plasma Nitriding and Nitrocarburising. *Materials* **2021**, *14*, 3320. [[CrossRef](#)]
31. Corujeira Gallo, S.; Dong, H. Study of Active Screen Plasma Processing Conditions for Carburising and Nitriding Austenitic Stainless Steel. *Surf. Coat. Technol.* **2009**, *203*, 3669–3675. [[CrossRef](#)]

**Disclaimer/Publisher’s Note:** The statements, opinions and data contained in all publications are solely those of the individual author(s) and contributor(s) and not of MDPI and/or the editor(s). MDPI and/or the editor(s) disclaim responsibility for any injury to people or property resulting from any ideas, methods, instructions or products referred to in the content.